Theor Chem Acc (2012) 131:1178
DOI 10.1007/s00214-012-1178-y

REGULAR ARTICLE

Variationally determined electronic states for the theoretical analysis of intramolecular interaction: I. Resonance energy and rotational barrier of the C–N bond in formamide and its analogs

Kenta Yamada · Nobuaki Koga

Received: 9 September 2011 / Accepted: 16 December 2011 / Published online: 21 March 2012

Abstract We present a new method that produces a variationally determined zeroth-order wave function for the analysis of intramolecular interactions between the fragments of a molecule. In our method, called the space-restricted wave function (SRW) method, this wave function is defined with nonorthogonal orbitals, which are obtained using the appropriately restricted variational spaces. The wave function thus obtained represents the electronic state with the target interactions deactivated, and it is constructed without unnecessarily breaking bonds, in contrast to some of the existing methods. Furthermore, we can perform energy decomposition analysis of intramolecular interactions using the zeroth-order functions that the SRW method yields. The validity of the SRW method is demonstrated in the analysis of the resonance energy and the rotational barrier of the C–N bond in formamide and its analogs. This method gives energy components that are different from those given by existing methods. With these components, we elucidate the origin of the rotational barrier from another point of view. Our SRW method gives meaningful results for the investigation of electron behavior and the nature of the molecular system.

Keywords Intramolecular interaction · Space-restricted wave function (SRW) method · Variationally determined zeroth-order wave function · Energy decomposition analysis (EDA) · In-plane/out-of-plane charge-transfer (CT) interaction · Molecular orbital (MO)-pair analysis

Electronic supplementary material The online version of this article (doi:10.1007/s00214-012-1178-y) contains supplementary material, which is available to authorized users.

K. Yamada · N. Koga (✉)
Graduate School of Information Science, Nagoya University, Furo-cho, Chikusa-ku, Nagoya 464-8601, Japan
e-mail: koga@is.nagoya-u.ac.jp

1 Introduction

Intermolecular and intramolecular interactions can account for the molecular properties of a system and the driving forces behind chemical reactions in the system. For instance, intramolecular interactions, such as conjugation, hyperconjugation, and resonance, are responsible for molecular conformation. It is reasonable to state that electronic information on intermolecular and intramolecular interactions is required to understand the nature of the system. Accordingly, a quantitative analysis of the interactions has been performed using various methods based on molecular orbital (MO) and density functional (DF) theories [1–42]. Analysis with these methods gives information on electronic processes accompanying the interactions in terms of a change in the electronic structure of the system, and the methods are expected to provide deeper insight into the interaction mechanisms.

A useful strategy for investigating the interactions is to calculate the interaction energy (E_{INT}.) that represents the change in total energy when the target interaction is activated (Eq. 1).

$$E_{\mathrm{INT}} = E_{0+\mathrm{INT}} - E_0, \tag{1}$$

where $E_{0+\mathrm{INT}}$ and E_0 are the total energies of electronic states with and without this interaction, respectively. The greatest difficulty in this strategy is defining the electronic state with the interaction deactivated, that is, the zeroth-order wave function, in agreement with chemical intuition. It follows that the energy of this wave function is E_0 in Eq. 1. In analyzing *intermolecular* interaction in an

interacting system, the wave function is easily defined as the product of each wave function of monomers isolated from each other, which make up the system. In analyzing *intramolecular* interaction, it is difficult to define the zeroth-order wave function because a molecule cannot be partitioned into well-defined fragments like monomers. The zeroth-order wave function must also be variationally determined to obtain qualitatively correct results. Consequently, several convenient methods are used for the analysis of intermolecular interaction, whereas relatively few methods are applied to the analysis of intramolecular interaction.

Energy decomposition analysis (EDA) can be carried out on the assumption that the interaction energy would be decomposed into various chemically meaningful energy components by using Eq. 1 successively. Each of these components originates from the characteristic behavior of electrons in the system, and thus, the EDA is expected to provide a clear picture of the interaction. Basically, the energy components of the total interaction energy between the kth and k'th fragments are attributed to the following four interactions, as shown in Scheme 1 [1]: (1) the classical electrostatic (ES) interaction between occupied MOs that are obtained when the fragments are isolated from each other; (2) the exchange (EX) interaction between occupied MOs, which causes a rearrangement of these MOs to result in destabilization; (3) the polarization (PL or POL) interaction that results in the mixing of the occupied space with the virtual space within each fragment under the influence of the other fragment; and (4) the charge-transfer (CT) interaction that causes interfragment delocalization by mixing the occupied space of one fragment with the virtual space of the other and vice versa.

The well-known methods for the EDA of *intramolecular* interactions may be classified into two main groups: (1) methods that give the energies of several components of the interaction (e.g., the Kitaura–Morokuma (KM) method [1, 2] and the Extended Transition State with the Natural Orbitals for Chemical Valence (ETS-NOCV) scheme [29]) and (2) methods that provide the energy of intramolecular CT interaction (e.g., the natural bond orbital deletion (NBO deletion) procedure [20], the block-localized wave function (BLW) technique [30–37], and the extremely localized molecular orbital (ELMO) approach [39, 40]). Some of these methods are outlined in the Supporting Information section.

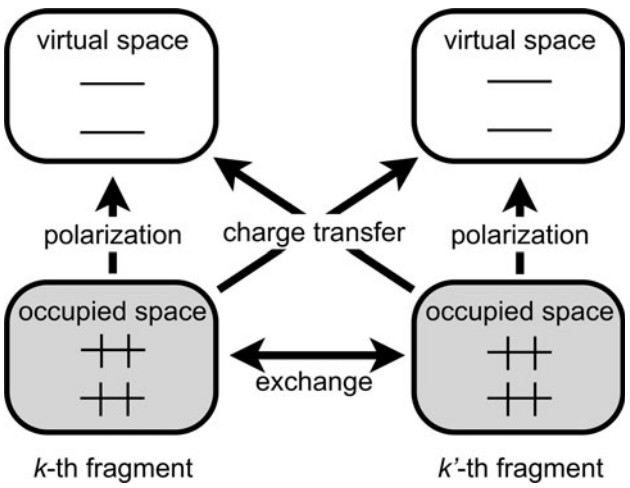

Scheme 1 Orbital interaction between fragments and various characteristic behaviors of electrons in this interaction

To overcome the limitations of zeroth-order wave functions in the well-known methods, we have developed a new method, namely, the space-restricted wave function (SRW) method, which provides a variationally determined zeroth-order wave function that is consistent with chemical intuition. This "fully relaxed" zeroth-order wave function is prepared without unnecessarily breaking bonds because this method is derived from the BLW method. Our zeroth-order wave function is obtained independently of molecular symmetry, in contrast to the BLW method, and it can be used for the analysis of various types of intramolecular interaction. The SRW method also gives several zeroth-order wave functions in which the removed intramolecular interactions are different from one another. These wave functions can be employed in the EDA of intramolecular interactions to estimate energy components that have meanings different from, for instance, the KM analysis. Thus, we analyze the intramolecular interaction from a different viewpoint. Therefore, the SRW method provides a useful way to investigate intramolecular interaction such that the behavior of electrons in the interaction is revealed. This would explain the difference in the nature between conformers, the nature of intramolecular hydrogen bonds, and the electronic effects of transition metals in complexes.

The SRW method has been developed under the Hartree–Fock (HF) approximation because the orbital concept is clearly defined (e.g., Koopmans' theorem) under this approximation, though the method can be easily extended with DF theory. It should be noted that we previously reported the prototype of the SRW method and used it to investigate intramolecular interactions in other molecules [43; our unpublished results]. This prototype had some deficiencies, but the present SRW method is a new method without these deficiencies and is much improved from the prototype.

We introduce the definitions of the electronic states mentioned above in the next section. In Sect. 3, the detailed applications of our SRW method for analyzing various types of intramolecular interaction are presented, with a discussion of the results and a comparison with the results of the BLW and KM methods under the HF approximation. Concluding remarks are given in Sect. 4.

2 Methodology

Initially, we define the space-restricted HF (SRHF) state, which plays a central role in our SRW technique. This state represents the most stable electronic state among the states where electrons are strictly localized in distinct regions of a molecule, and it is used to estimate the effects of intramolecular interaction, such as the CT interaction, caused by an orbital overlap. The following indices are used throughout the paper: μ, ν are basis function indices; i, j are occupied MO indices; a, b are virtual MO indices; and k, k' (k' is not identical to k unless otherwise specified) are the subspace indices. In this paper, the SRW formulation for a closed shell with an even number of electrons is presented and that for an open shell can be constructed in a straightforward manner.

2.1 The SRHF state

For a closed-shell molecule with N electrons and M basis functions $\boldsymbol{\chi} = (\chi_1 \ \cdots \ \chi_\nu \ \cdots \ \chi_M)$, let us assume that the entire space provided by M basis functions is partitioned into K subspaces. Then, the kth subspace $(k = 1, 2, \ldots, K)$ is spanned by m^k ($\leq M$) basis functions in the kth subset of M basis functions, $\boldsymbol{\chi}^k = (\chi^k_1 \ \cdots \ \chi^k_\mu \ \cdots \ \chi^k_{m^k})$. MOs expanded in the kth subspace thus defined are called k-SRMOs; these are used to represent an electronic structure of the kth fragment, such as a functional group and a bond or a set of groups and/or bonds. However, upon an intramolecular interaction, the electronic structure of the kth fragment involved directly in this interaction is not completely represented by k-SRMOs. This is because k-SRMOs do not have tails as a result of interactions with other orbitals: interaction and orthogonalization tails, which are included in standard localized MOs (LMOs) [44–47], derived from the HF wave function. A space spanned by such tails is outside of the kth subspace and thus is called unused space Δ^k_{tails}. This unused space is described by the basis functions not included in the kth subset, and the set constituted of these basis functions is called $\boldsymbol{\delta}^k_{\text{tails}}$.

The n^k_{o} lower-energy k-SRMOs occupied by $2n^k_{\text{o}}$ electrons (occupied k-SRMOs; $N = \sum_{k=1}^{K} 2n^k_{\text{o}}$) and n^k_{v} $\left(\leq m^k - n^k_{\text{o}}\right)$ k-SRMOs (virtual k-SRMOs) are defined as

$$\begin{aligned}\boldsymbol{\varphi}^k_{\text{o}} &= \left(\varphi^k_1 \ \cdots \ \varphi^k_i \ \cdots \ \varphi^k_{n^k_{\text{o}}}\right) \\ &= \boldsymbol{\chi}^k \mathbf{C}^k \end{aligned} \tag{2}$$

and

$$\begin{aligned}\boldsymbol{\varphi}^k_{\text{v}} &= \left(\varphi^k_{n^k_{\text{o}}+1} \ \cdots \ \varphi^k_{n^k_{\text{o}}+a} \ \cdots \ \varphi^k_{n^k_{\text{o}}+n^k_{\text{v}}}\right) \\ &= \boldsymbol{\chi}^k \mathbf{B}^k, \end{aligned} \tag{3}$$

respectively. With Eq. 2, the occupied SRMO coefficient matrix $\mathbf{T}$ is obtained as follows:

$$\begin{aligned}\boldsymbol{\varphi}_{\text{o}} &= \left(\boldsymbol{\varphi}^1_{\text{o}} \ \cdots \ \boldsymbol{\varphi}^k_{\text{o}} \ \cdots \ \boldsymbol{\varphi}^K_{\text{o}}\right) \\ &= \left(\boldsymbol{\chi}^1 \ \cdots \ \boldsymbol{\chi}^k \ \cdots \ \boldsymbol{\chi}^K\right)\left(\mathbf{C}^1 \ \cdots \ \mathbf{C}^k \ \cdots \ \mathbf{C}^K\right) \\ &= \left(\chi_1 \ \cdots \ \chi_\nu \ \cdots \ \chi_M\right)\left(\mathbf{T}^1 \ \cdots \ \mathbf{T}^k \ \cdots \ \mathbf{T}^K\right) \\ &= \boldsymbol{\chi}\mathbf{T}, \end{aligned} \tag{4}$$

where $\mathbf{T}^k$ is the $M \times n^k_{\text{o}}$ matrix represented by

$$T^k_{\nu i}\begin{cases} = C^k_{\mu i} & \left(\chi_\nu \in \left\{\chi^k_\mu; \mu = 1, \ldots, m^k\right\}\right) \\ = 0 & \left(\chi_\nu \notin \left\{\chi^k_\mu; \mu = 1, \ldots, m^k\right\}\right) \end{cases}, \tag{5}$$

and $\mathbf{T}$ is then the $M \times N/2$ matrix. $\mathbf{T}^k$ gives the SRW orthonormalization condition for the occupied k-SRMOs:

$$\mathbf{T}^{k+}\mathbf{S}\mathbf{T}^{k'}\begin{cases} = \mathbf{1} & (k = k') \\ \neq \mathbf{0} & (k \neq k'), \end{cases} \tag{6}$$

in which the superscript "+" denotes the transpose operation and $\mathbf{S}$ is the overlap matrix of all the basis functions. Note that in Eq. 4, some or all of the basis functions in the kth subset can be used in different subsets. This is a major difference between our method and the BLW method. Although it is possible that the SRHF state is in agreement with the BLW state when $M \geq \sum_{k=1}^{K} m^k$, this case is less likely to occur in an analysis of intramolecular interaction because one of the basis functions in a molecule is usually shared among several fragments.

Using occupied SRMOs, the SRHF state is defined through a Slater determinant:

$$\begin{aligned}\Psi_{\text{SRHF}} = \hat{A}\Big\{&\varphi^1_1\bar{\varphi}^1_1\varphi^1_2\bar{\varphi}^1_2\cdots\varphi^1_{n^1_{\text{o}}}\bar{\varphi}^1_{n^1_{\text{o}}}\cdots\varphi^k_1\bar{\varphi}^k_1\varphi^k_2\bar{\varphi}^k_2\cdots\varphi^k_{n^k_{\text{o}}}\bar{\varphi}^k_{n^k_{\text{o}}} \\ &\cdots\varphi^K_1\bar{\varphi}^K_1\varphi^K_2\bar{\varphi}^K_2\cdots\varphi^K_{n^K_{\text{o}}}\bar{\varphi}^K_{n^K_{\text{o}}}\Big\} = \hat{A}\left\{\Phi^1\cdots\Phi^k\cdots\Phi^K\right\}, \end{aligned} \tag{7}$$

where $\hat{A}$ is the antisymmetrizer and Φ^k is the product of occupied k-SRMOs. For simplicity, the normalization factor depending on the number of electrons and overlap integrals between occupied k- and k'-SRMOs is omitted in Eq. 7 and in the following discussion. Furthermore, the SRHF state thus defined is not an eigenstate of the Hamiltonian. The energy formula of the SRHF state is expressed by the following equation:

$$E_{\text{SRHF}} = \text{Tr}[\mathbf{D}\mathbf{H}_{\text{core}}] + \text{Tr}[\mathbf{D}\mathbf{F}(\mathbf{D})] + E_{\text{nuc}}, \tag{8}$$

where $\mathbf{H}_{\text{core}}$ is the core Hamiltonian matrix, $\mathbf{D}$ is the density matrix[1] defined as

$$\mathbf{D} = \mathbf{T}(\mathbf{T}^+\mathbf{S}\mathbf{T})^{-1}\mathbf{T}^+, \tag{9}$$

[1] The density matrix used in the SRW approach is half of that usually defined in the HF scheme.

$\mathbf{F}(\mathbf{D})$ is the Fock matrix, and E_{nuc} is the nuclear repulsion energy.

2.2 The fully relaxed SRHF state

We now explain how to lead the total energy E_{SRHF} to a stationary point with regard to $\mathbf{T}$, which corresponds to the fully relaxed SRHF state.

2.2.1 Initial occupied SRMOs

First, we prepare initial occupied k-SRMOs $\boldsymbol{\varphi}^{0,k} = \boldsymbol{\chi}\mathbf{T}^{0,k}$ by removing $\Delta^k_{\mathrm{tails}}$ from occupied natural localized MOs (NLMOs) [47], given as

$$\begin{aligned}\boldsymbol{\phi} &= \begin{pmatrix}\phi_1 & \cdots & \phi_l & \cdots & \phi_{N/2}\end{pmatrix} \\ &= \boldsymbol{\chi}\mathbf{L}.\end{aligned} \tag{10}$$

This is done by zeroing out the coefficients of the basis functions constituting $\boldsymbol{\delta}^k_{\mathrm{tails}}$ in the several NLMOs, which represent the electronic structure of the kth fragment, and by orthonormalizing the remaining coefficients (see Appendix 1 for the detailed derivation of initial occupied k-SRMOs). One of the reasons why NLMOs are employed in our approach is that they conveniently provide the qualitative features of the orbitals related directly and indirectly to a target interaction.[2]

2.2.2 Initial virtual SRMOs

Next, candidates for initial virtual k-SRMOs are given by the orthonormalization of all the k-SRMOs with respect to initial occupied k-SRMOs $\boldsymbol{\varphi}^{0,k}_{\mathrm{o}}$ (Eq. 11).

$$\begin{aligned}\tilde{\boldsymbol{\varphi}}^{0,k}_{\mathrm{v}} &= \begin{pmatrix}\tilde{\varphi}^{0,k}_{n^k_{\mathrm{o}}+1} & \cdots & \tilde{\varphi}^{0,k}_{n^k_{\mathrm{o}}+a} & \cdots & \tilde{\varphi}^{0,k}_{n^k_{\mathrm{o}}+\tilde{n}^k_{\mathrm{v}}}\end{pmatrix} \\ &= \boldsymbol{\chi}^k\tilde{\mathbf{B}}^{0,k} = \boldsymbol{\chi}\tilde{\mathbf{X}}^{0,k},\end{aligned} \tag{11}$$

where $\tilde{n}^k_{\mathrm{v}}$ is the number of these candidates, which is equal to $m^k - n^k_{\mathrm{o}}$, and $\tilde{\mathbf{X}}^k$ is the provisional matrix of $\mathbf{X}^k$ for virtual k-SRMOs, which corresponds to $\mathbf{T}^k$ for occupied k-SRMOs. There can be three notable types of the subspaces according to the relation between the basis functions of one of the subsets (say, the kth subset) and the other subset (say, the k'th subset), as shown schematically in Scheme 2[3]: (1) the basis functions in the kth subset are not used in the k'th subset under the condition that (a) all SRMOs of the kth subset have a symmetry different from those of the k'th subset or (b) all SRMOs of the kth subset have the same symmetry as those of the k'th subset; (2) the basis functions in the kth subset are identical to all the basis functions (i.e., $m^k = M$); (3) the basis functions in the kth subset are entirely used in the k'th subset (i.e., $\left\{\chi^k_\mu; \mu = 1, \ldots, m^k\right\} \subset \left\{\chi^{k'}_\nu; \nu = 1, \ldots, m^{k'}\right\}$).

In the type 1 kth subspace, initial virtual k-SRMOs are obtained from the following equation with the candidates (Eq. 11):

$$\begin{aligned}\boldsymbol{\varphi}^{0,k}_{\mathrm{v}} &= \boldsymbol{\chi}\tilde{\mathbf{X}}^{0,k}\mathbf{N}^{0,k}_{\mathrm{v1}} \\ &= \boldsymbol{\chi}\mathbf{X}^{0,k},\end{aligned} \tag{12}$$

in which $\mathbf{N}^{0,k}_{\mathrm{v1}}$ is the diagonal matrix with the normalization factors (henceforth called the normalization matrix). This equation indicates that the candidates mentioned above are used as initial virtual orbitals as is. While the normalization matrix in the equation is not necessary, for consistency with the following equations, the unit matrix $\mathbf{N}^{0,k}_{\mathrm{v1}}$ is added. Next, in the type 2 kth subspace, initial virtual k-SRMOs are derived from the candidates with occupied NLMOs (Eq. 10) so as not to compensate for $\Delta^{k'}_{\mathrm{tails}}(k' = 1, 2, \cdots, k-1, k+1, \ldots, K)$, as given below.

$$\begin{aligned}\boldsymbol{\varphi}^{0,k}_{\mathrm{v}} &= \boldsymbol{\chi}(\mathbf{1} - \mathbf{L}\mathbf{L}^{+}\mathbf{S})\tilde{\mathbf{X}}^{0,k}\mathbf{N}^{0,k}_{\mathrm{v2}} \\ &= \boldsymbol{\chi}\mathbf{X}^{0,k},\end{aligned} \tag{13}$$

in which $\mathbf{N}^{0,k}_{\mathrm{v2}}$ is the normalization matrix. In the type 3 kth subspace, initial virtual k-SRMOs are generated from the candidates with the following projection to avoid replacing occupied k-SRMOs with occupied k'-SRMOs during our SCF procedure:

$$\begin{aligned}\boldsymbol{\varphi}^{0,k}_{\mathrm{v}} &= \boldsymbol{\chi}\left(\mathbf{1} - \mathbf{T}^{0,k}_{\mathrm{p}}\mathbf{T}^{0,k+}_{\mathrm{p}}\mathbf{S}\right)\tilde{\mathbf{X}}^{0,k}\mathbf{N}^{0,k}_{\mathrm{v3}} \\ &= \boldsymbol{\chi}\mathbf{X}^{0,k}.\end{aligned} \tag{14}$$

In this equation, $\mathbf{N}^{0,k}_{\mathrm{v3}}$ is the normalization matrix and $\mathbf{T}^{0,k}_{\mathrm{p}}$ is the coefficient matrix of pseudo-occupied k-SRMOs, $\boldsymbol{\varphi}^{0,k}_{\mathrm{p}}$, which are obtained by restricting occupied k'-SRMOs within the kth subspace (see Appendix 2 for the detailed derivation). The projection procedures in Eqs. 13 and 14 eliminate some portions of the virtual parts in the type 2 and 3 kth subspaces, respectively (eliminated parts: green areas in Scheme 2). In other types of the kth subspace, initial virtual k-SRMOs are prepared in the same manner as in the type 1 kth subspace. Note that the BLW method can

[2] In addition to the reason mentioned here, it is highly probable that the NLMOs are given in any structure, even if a molecular structure is significantly different from the HF structure, because they are generated not directly from the unitary transformation of the canonical MOs but from the natural atomic orbitals (NAO) prepared by partitioning the density matrix. Furthermore, the NLMOs are much less sensitive to the chosen basis set than LMOs produced by other methods. See http://www.chem.wisc.edu/~nbo5 and the literature mentioned therein.

[3] When very large basis sets are employed, it would be necessary to place additional restrictions on the kth subspace.

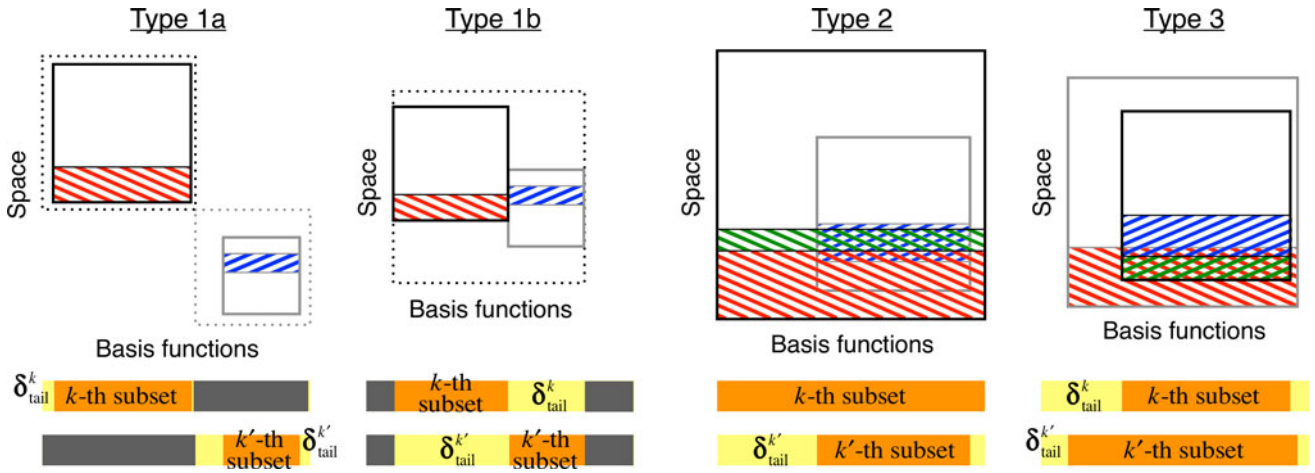

Scheme 2 Relation between the basis functions in the kth and k'th subsets when orbitals described by all the basis functions have only two symmetries. In this scheme, *red* or *blue*, *white*, and *green* areas represent occupied, virtual, and eliminated parts, respectively, in the subspace. Furthermore, *dotted boxes* show that in the type 1a, k- and k'-SRMOs have different symmetries and that in the type 1b, k- and k'-SRMOs have the same symmetry. The *orange* and *yellow* areas indicate the basis functions describing the subspaces and unused spaces, respectively (see details in the text), and the *gray* areas represent the basis functions that cannot describe the subspaces or unused spaces in terms of the symmetry

produce the fully relaxed BLW state only when the subspaces are entirely type 1.

2.2.3 The SCF procedure

After the occupied and virtual parts of every subspace are clearly defined by the above-mentioned initialization, the occupied part of each subspace is varied to provide the lower SRHF energy (Eq. 8) by using the virtual part of the same subspace. In this study, we employ the SCF procedure (which differs from those used in other approaches [30, 38, 39]); this procedure diagonalizes a modified Fock matrix for every occupied SRMO in order to preserve its *localized* shape, as shown in the Supporting Information section. Note that to prioritize the change in the occupied SRMOs described by fewer basis functions, our iteration procedure is performed in the kth subspace in advance of the k'th subspace when $m^k < m^{k'}$. This is done because these SRMOs probably would vary more significantly from NLMOs than would the occupied SRMOs described by more basis functions.

2.3 EDA with the SRW method

When the electronic state in which all the subspaces are isolated from each other (subspace-isolated HF, SIHF state) is defined, the total inter-subspace interaction energy is calculated as the difference between the energy of this state and that by the conventional HF method. Furthermore, with various electronic states including the space-restricted Hartree product (SRHP) state and the SRHF state, which are obtained by activating only a selected interaction successively from the SIHF state, the total interaction energy can be decomposed, as done in the existing EDA methods. In this subsection, the EDA scheme using these states is presented.

2.3.1 The SIHF state

The SIHF state is determined using occupied MOs expanded in the isolated subspaces (subspace-isolated MOs, SIMOs), and these subspaces are also composed of virtual SIMOs. The total interaction energy between the subspaces is given using this state as the zeroth-order wave function.

$$E_{\text{INT}} = E_{\text{HF}} - E_{\text{SIHF}}, \tag{15}$$

where E_{SIHF} is the energy of the SIHF state.

$$E_{\text{SIHF}} = \sum_{k=1}^{K} \left\{ \text{Tr}\left[\mathbf{D}'^k \mathbf{H}^k_{\text{core}}\right] + \text{Tr}\left[\mathbf{D}'^k \mathbf{F}^k\left(\mathbf{D}'^k\right)\right] + E^k_{\text{nuc}} \right\}, \tag{16}$$

where $\mathbf{D}'^k$ and $\mathbf{F}^k\left(\mathbf{D}'^k\right)$ are the density and Fock matrices, respectively, calculated using the occupied SIMOs in the kth subspace (occupied k-SIMOs $\left\{\varphi'^k_i; i = 1, 2, \ldots, n^k_{\text{o}}\right\}$); $\mathbf{H}^k_{\text{core}}$ and E^k_{nuc} are the core Hamiltonian matrix and nuclear repulsion energy, respectively, for the kth isolated subspace. In other words, E_{SIHF} is the sum of the energies for each noninteracting subspace.

2.3.2 The SRHP state

Next, we present the definition of another state in the SRW method, namely, the SRHP state. This electronic state is designed to estimate EX interaction between different

subspaces, and thus, it is expressed as the Hartree product (HP) of the Slater determinants $\hat{A}\{\Phi'^k\}$, each of which is composed of the occupied k-SIMOs.

$$\Psi_{\mathrm{SRHP}} = \hat{A}\{\Phi'^1\}\cdots\hat{A}\{\Phi'^k\}\cdots\hat{A}\{\Phi'^K\}. \tag{17}$$

The energy formula for this state is

$$E_{\mathrm{SRHP}} = 2\mathrm{Tr}\left[\mathbf{D}'_{\mathrm{sum}}\mathbf{H}_{\mathrm{core}}\right] + \sum_{k=1}^{K}\left\{\mathrm{Tr}\left[\mathbf{D}'^k\mathbf{G}\left(\mathbf{D}'^k\right)\right] + \sum_{k'\neq k}^{K}\mathrm{Tr}\left[\mathbf{D}'^k\mathbf{J}\left(\mathbf{D}'^k\right)\right]\right\} + E_{\mathrm{nuc}}, \tag{18}$$

where $\mathbf{D}'_{\mathrm{sum}}$ is the density matrix for the whole system that is composed of the subspaces:

$$\mathbf{D}'_{\mathrm{sum}} = \sum_{k=1}^{K}\mathbf{D}'^k. \tag{19}$$

$\mathbf{G}\left(\mathbf{D}'^k\right)$ is the two-electron integral matrix for the kth subspace, and $\mathbf{J}\left(\mathbf{D}'^k\right)$ is the Coulomb integral matrix for evaluating the Coulomb interaction between occupied k-SIMOs and k'-SIMOs.

The EX interaction can be decomposed into two interactions, namely, electron-exchange (EE) interaction and Pauli repulsion. The former and the latter originate from the impossibility of distinguishing electrons and the Pauli exclusion principle, respectively. Furthermore, Pauli repulsion contributes to the destabilization of the system associated with the distortion in electron density to eliminate an orbital overlap between occupied k-SIMOs. Following the concept of the EDA, we assume two processes: (1) only EE interaction is activated in the SRHP state and (2) Pauli repulsion is activated, in addition to EE interaction in the SRHP state. Accordingly, the energy of the state representing the first process is written as

$$E_{\mathrm{SRHP+EE}} = \mathrm{Tr}\left[\mathbf{D}'_{\mathrm{sum}}\mathbf{H}_{\mathrm{core}}\right] + \mathrm{Tr}\left[\mathbf{D}'_{\mathrm{sum}}\mathbf{F}\left(\mathbf{D}'_{\mathrm{sum}}\right)\right] + E_{\mathrm{nuc}}, \tag{20}$$

and the energy of the state with the second process is given as

$$E_{\mathrm{SRHP+EE+Pauli}} = E_{\mathrm{SRHP+EX}} = \mathrm{Tr}[\mathbf{D}'\mathbf{H}_{\mathrm{core}}] + \mathrm{Tr}[\mathbf{D}'\mathbf{F}(\mathbf{D}')] + E_{\mathrm{nuc}}, \tag{21}$$

where $\mathbf{D}'$ is the density matrix calculated by Eq. 9 using occupied SIMOs. The SRHP state is then viewed as the state where POL interaction within each subspace, as well as the inter-subspace EX interaction, is eliminated from the SRHF state.

2.3.3 Energy components

Using the above-mentioned energies, the SRW method enables us to obtain the energy components of the total interaction energy (the SRW decomposition scheme).

$$\begin{aligned} E_{\mathrm{INT}} &= E_{\mathrm{ES}} + E_{\mathrm{EX}} + E_{\mathrm{POL}} + E_{\mathrm{CT}} \\ &= E_{\mathrm{ES}} + E_{\mathrm{EE}} + E_{\mathrm{Pauli}} + E_{\mathrm{POL}} + E_{\mathrm{CT}}. \end{aligned} \tag{22}$$

In this scheme, the EX, POL, and CT interaction energies are expressed in terms of the energy change (Eq. 1):

$$E_{\mathrm{EX}} = E_{\mathrm{SRHP+EX}} - E_{\mathrm{SRHP}}, \tag{23}$$

$$E_{\mathrm{POL}} = E_{\mathrm{SRHF}} - E_{\mathrm{SRHP+EX}}, \tag{24}$$

and

$$E_{\mathrm{CT}} = E_{\mathrm{HF}} - E_{\mathrm{SRHF}}, \tag{25}$$

respectively. E_{SRHF} in Eq. 24 is calculated with the occupied and virtual SIMOs via the SCF procedure in Sect. 2.2.3. E_{EX} would be further partitioned into the two components, that is, EE interaction energy (E_{EE}) and Pauli repulsion energy (E_{Pauli}):

$$E_{\mathrm{EE}} = E_{\mathrm{SRHP+EE}} - E_{\mathrm{SRHP}} \tag{26}$$

and

$$E_{\mathrm{Pauli}} = E_{\mathrm{SRHP+EX}} - E_{\mathrm{SRHP+EE}}. \tag{27}$$

ES interaction energy (E_{ES}), which usually becomes very large, is presented with E_{SIHF}:

$$E_{\mathrm{ES}} = E_{\mathrm{SRHP}} - E_{\mathrm{SIHF}}. \tag{28}$$

It is generally not appropriate to use the initial occupied and virtual SRMOs, defined in Sects. 2.2.1 and 2.2.2, as the SIMOs in the analysis of the total intramolecular interaction because these already include the contributions of all interaction components except that of the CT interaction between the subspaces. However, in this paper, we used the initial SRMOs to represent the zeroth-order wave function for E_{INT}, as justified later; E_{SRHF} in Eqs. 24 and 25 was obtained via the SCF procedure starting from the initial SRMOs, though it would be slightly different from that with the SIMOs. Then, details regarding the SIHF state and SIMOs will be published in the third paper in this series.

3 Applications: formamide and its analogs

To demonstrate the usefulness of our SRW method and to compare our results for intramolecular interaction with those of other methods, we analyzed the resonance energy and the rotational barrier of the C–N bond in formamide and its analogs (vinylamine, formamidine, and thioformamide) [48–68]. In the current study, the Gaussian 03 suite

of programs [69] is used to carry out the standard SCF calculations, to form the NLMOs [70] and to compute the one- and two-electron integrals required for performing the SRW calculations. The NLMOs assigned to the inner shells of the constituent atoms of the molecules were kept unchanged throughout all the SRW calculations (frozen-core approximation) because they would only slightly affect the target intramolecular interactions.

It is important to examine the structure of formamide, in particular because this molecule is the simplest model for mimicking the backbone peptide group in proteins [48–51]. Thus, to gain insight into the electronic property of the peptide bond, we studied the resonance and the internal rotation around the C–N bond in formamide and it analogs. For comparison with the previous analysis using the BLW method [32], the following calculations were carried out with the 6-31G(d) basis set [71–73], which gives reliable rotational barriers of formamide and thioformamide [32].

3.1 Resonance effect

The resonance in formamide in the planar conformation has been discussed in terms of the Lewis structures shown in Scheme 3 (X=O), and it is represented by I ↔ II ↔ III [32, 48, 49, 51–61]. Let us evaluate the effect of the resonance on the character of the C–N bond by calculating the state in which Lewis structure III is eliminated from the HF state, and thus, the N lone-pair electrons and C=O π bonding electrons localize the N atom and the C=O bonding region, respectively. Comparison of such a state with the HF state would give information on the electron delocalization from the lone pair on the N atom to the carbonyl π* orbital.

In the planar structure optimized at the HF/6-31G(d) level of theory (henceforth called structure **A**), the vertical resonance energy (VRE) is obtained as

$$\begin{aligned} E_{\mathrm{VRE}} &= E_{0+\mathrm{VRE}} - E_0 \\ &= E\left(\Psi^{\mathbf{A}}_{\mathrm{HF}}\right) - E\left(\Psi^{\mathbf{A}}_{\mathrm{SRHF}}\right), \end{aligned} \tag{29}$$

where $\Psi^{\mathbf{A}}_{\mathrm{HF}}$ and $\Psi^{\mathbf{A}}_{\mathrm{SRHF}}$ are the wave functions of structure **A** without and with the elimination of Lewis structure III, respectively, as given below:

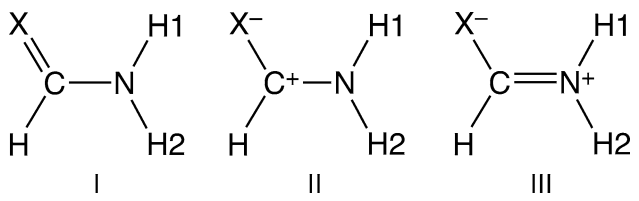

Scheme 3 The main three Lewis structures related to three π-type atomic orbitals and four π electrons that contribute to the resonance interaction in formamide and its analogs

$$\Psi^{\mathbf{A}}_{\mathrm{HF}} = \hat{A}\left(\Phi^{\mathbf{A}}_{\sigma_{\mathrm{HF}}}\phi^{\mathbf{A}}_{\pi_{\mathrm{CO}}}\phi^{\mathbf{A}}_{\mathrm{n_N}}\right) \tag{30}$$

$$\Psi^{\mathbf{A}}_{\mathrm{SRHF}} = \hat{A}\left(\Phi^{\mathbf{A}}_{\sigma}\varphi^{\mathbf{A}}_{\pi_{\mathrm{CO}}}\varphi^{\mathbf{A}}_{\mathrm{n_N}}\right). \tag{31}$$

In these equations, the symbol σ stands for the σ-skeleton of this conformer; the π_{CO} and $\mathrm{n_N}$ denote the carbonyl π and N lone pair orbitals, respectively; and $\Phi_{\sigma_{\mathrm{HF}}}$ and Φ_{σ} represent the Hartree product of the occupied NLMOs and SRMOs corresponding to the σ-skeleton, respectively. Note that in $\Psi^{\mathbf{A}}_{\mathrm{SRHF}}$, the resonance between I and II is taken into account.

In an analysis of π interaction in the *planar* structure, the SRHF state ($\Psi^{\mathbf{A}}_{\mathrm{SRHF}}$) is equivalent to the BLW state because in this case the basis functions spanning each subspace are included in one and only one subset (see Type 1 in Scheme 2). As a result, E_{VRE} and also the adiabatic resonance energy (ARE), which is the variation in energy between $\Psi^{\mathbf{A}}_{\mathrm{HF}}$ and the SRHF state of the planar geometry optimized without the resonance interaction (planar SRHF structure), are the same as those determined by the BLW method ($E_{\mathrm{VRE}} = 25.50$ and $E_{\mathrm{ARE}} = 22.48$ kcal/mol) [32]. Although the electron density in the SRHF state (Eq. 9) and that in the BLW state are the same in this situation, with the SRHF state, an MO-pair analysis (described in the following paragraphs) can be performed because there is one-to-one correspondence between the SRMO and NLMO, which are regarded as a *pair*.

Figure 1 shows the two SRMOs $\varphi^{\mathbf{A}}_{\pi_{\mathrm{CO}}}$ and $\varphi^{\mathbf{A}}_{\mathrm{n_N}}$ as well as their parent NLMOs (i.e., $\phi^{\mathbf{A}}_{\pi_{\mathrm{CO}}}$ and $\phi^{\mathbf{A}}_{\mathrm{n_N}}$). This illustrates that while $\varphi^{\mathbf{A}}_{\pi_{\mathrm{CO}}}$ is allowed to be closer to the amino group by the absence of the orthogonalization among the SRMOs, it resembles $\phi^{\mathbf{A}}_{\pi_{\mathrm{CO}}}$, reflecting the small amount of interaction between the π_{CO} orbital and the $\mathrm{n_N}$ orbital, and also it indicates that $\varphi^{\mathbf{A}}_{\mathrm{n_N}}$ is highly localized on the N atom, unlike $\phi^{\mathbf{A}}_{\mathrm{n_N}}$, which has a significant delocalization tail originating mainly from the π^{*}_{CO} orbital, in addition to the orthogonalization tail. This confirms that these SRMOs accurately represent the behavior of π electrons when the resonance interaction is absent.

To further explain the difference between these SRMOs and NLMOs, we here present an alternative view in terms of the difference electron density (DED). The DED in the Löwdin basis (DED-LB) between the *i*th occupied SRMO (φ_i) and its parent NLMO (ϕ_i), $\Delta\rho_i$, is

$$\Delta\rho_i = \rho[\phi_i] - \rho[\varphi_i]. \tag{32}$$

In this equation, $\rho[\phi_i]$ and $\rho[\varphi_i]$ are the electron densities of ϕ_i and φ_i in the Löwdin basis, respectively (see Supporting Information for details). The DED-LB thus obtained can be diagonalized by a unitary matrix [74, 75]. This procedure gives a kind of natural orbitals [76], and the unitary matrix

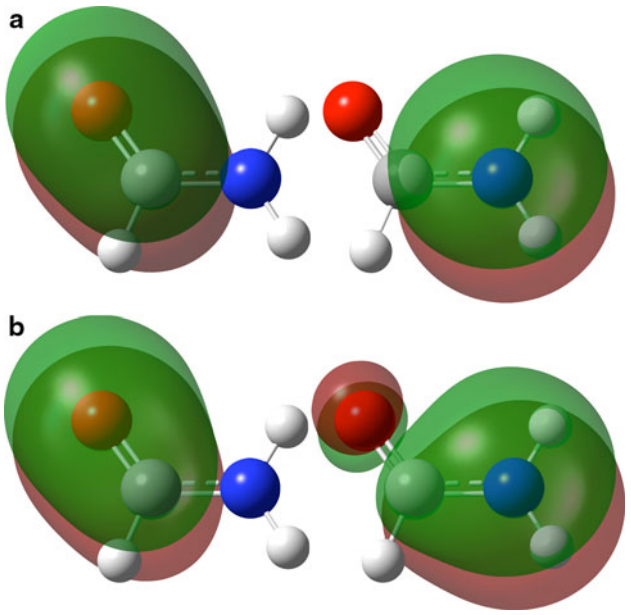

Fig. 1 Occupied **a** SRMOs and **b** NLMOs exhibiting π_{CO} and n_N orbitals (*left* and *right*, respectively) in formamide. The isosurface value is 0.02

corresponds to the coefficient matrix for those orbitals, known as the DEDLB-derived natural orbitals (DDNOs) in the Löwdin basis. Then, the DED-LB is represented as

$$\Delta\rho_i = |\lambda_i|\left\{(\Delta\psi_{+i})^2 - (\Delta\psi_{-i})^2\right\}, \tag{33}$$

in which $\Delta\psi_{+i}$ and $\Delta\psi_{-i}$ are the eigenvectors of $\Delta\rho_i$ associated with the eigenvalues λ_i and $-\lambda_i$, respectively. The electron densities of the complementary DDNOs, $(\Delta\psi_{+i})^2$ and $(\Delta\psi_{-i})^2$, with the weighting factor $|\lambda_i|$, indicate the *characteristic* parts of $\rho[\phi_i]$ and $\rho[\varphi_i]$. Furthermore, in light of the Löwdin basis, $|\lambda_i|$ coincides with the number of electrons that flow from $\Delta\psi_{-i}$ to $\Delta\psi_{+i}$.

The DED-LB map between $\phi^{\mathbf{A}}_{n_N}$ and $\varphi^{\mathbf{A}}_{n_N}$ ($\Delta\rho_{n_N}$), together with $|\lambda_{n_N}|(\Delta\psi_{+n_N})^2$ and $-|\lambda_{n_N}|(\Delta\psi_{-n_N})^2$, is presented in Fig. 2. This figure shows that electrons flow from the n_N to the π^*_{CO} orbital and that, judging from the nodal property, $\Delta\psi^{\mathbf{A}}_{+n_N}$ and $\Delta\psi^{\mathbf{A}}_{-n_N}$ can be considered as the CN π-*bonding* orbital and its *antibonding* counterpart having the lone pair character, respectively. Accordingly, this electron flow (0.428 *e*) leads to an increase of the π-electron density between the C and N atoms and to a decrease of that in the nitrogen lone pair, thereby contributing to the resonance effect. Note that the complementary DDNOs thus obtained require the presence of the orthogonalization tails because they must be orthogonal. Because the present complementary DDNOs have large tails like canonical MOs, more localized DDNOs would lead to easier interpretation of the change in electronic state. We will present a method that

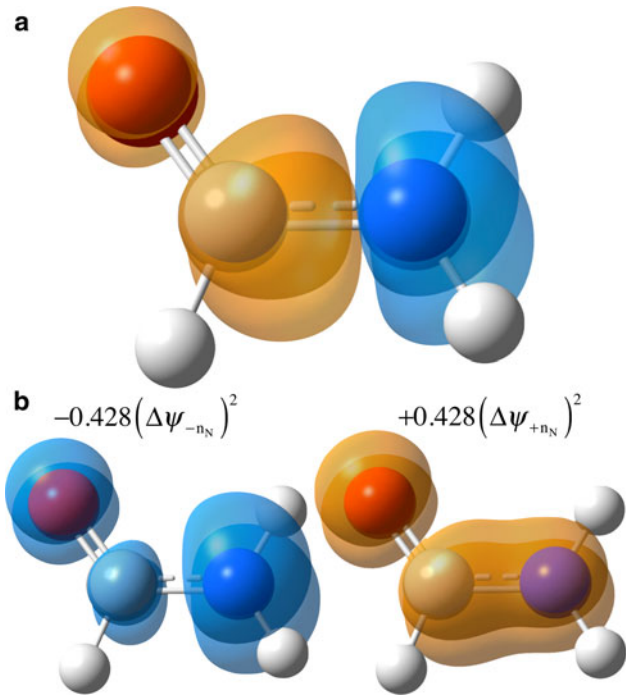

Fig. 2 **a** The DED-LB map for the $n_N \rightarrow \pi^*_{CO}$ interaction and **b** the weighted densities of the complementary DDNOs obtained from the DED-LB in the planar HF structure (structure **A**) of formamide. In this figure, the lobes in aqua and orange denote a decrease and an increase, respectively, of the electron density. The isosurface values are 0.002 *e*/bohr^3

gives well-localized DDNOs in a subsequent paper in this series.

3.2 Rotational barrier

The amide group is one of the key functional groups in chemistry. Its planarity and relatively high barrier to rotation about the C–N bond could be dominant factors in determining the conformations of peptides and related compounds. By deleting the resonance in structure **A** corresponding to the ground-state conformer, the planar SRHF structure (structure **B**) is obtained (as mentioned above in relation to estimating E_{ARE}), and this accurately reflects the deletion of this interaction, which results in a longer C–N bond and a shorter C=O bond (Table 1). Analogous to the SRHF state of structure **A** (Eq. 31), the SRHF state of structure **B** can be represented as

$$\Psi^{\mathbf{B}}_{SRHF} = \hat{A}\left(\Phi^{\mathbf{B}}_{\sigma}\varphi^{\mathbf{B}}_{\pi_{CO}}\varphi^{\mathbf{B}}_{\backslash_N}\right). \tag{34}$$

In conjunction with the resonance interaction, the in-plane CT interaction between the formyl and amino groups could contribute to the rotational barrier. The additional deactivation of these σ-type interactions yields the SRHF state of another planar SRHF structure (structure **C**), the parameters of which are listed in Table 1.

Table 1 Structures of formamide conformers determined at the SRHF/6-31G(d) level (structures **B** to **E**) and the HF/6-31G(d) level (Structures **A**, **F**, **G1**, and **G2**)

Structural parameter	Structure								
	A	**B**	**C**	**D**	**E**	**F**	**G1**	**G2**	**G3**[a]
Bond length [Å]									
C–H	1.091	1.089	1.086	1.086	1.083	1.091	1.087	1.095	1.087
C=O	1.193	1.176	1.175	1.175	1.175	1.182	1.183	1.179	1.183
C–N	1.348	1.420	1.438	1.438	1.463	1.405	1.427	1.422	1.427
N–H1	0.996	0.992	0.990	0.990	0.990	0.993	1.005	1.005	1.005
N–H2	0.993	0.990	0.989	0.989	0.990	0.993	1.005	1.005	1.005
Bond angle [degrees]									
∠O–C–H	122.3	123.2	123.7	123.7	122.3	120.0	121.5	120.4	121.5
∠N–C–O	125.0	124.0	123.5	123.5	123.6	124.6	125.1	123.2	125.1
∠H1–N–C	119.3	118.9	119.1	119.1	120.4	120.8	108.5	109.8	108.5
∠H2–N–C	121.8	121.3	121.0	121.0	120.4	120.8	108.5	109.8	108.5
Dihedral angle [degrees]									
∠H1–N–C–O	0.0	0.0	0.0	90.0	90.0	90.0	57.1	121.7	122.9
∠H2–N–C–O	180.0	180.0	180.0	−90.0	−90.0	−90.0	−57.1	−121.7	−122.9

The dihedral angle ∠N–C–O–H is fixed to 180.0° throughout the amino group rotation in formamide

The schematic structures and the atom numbering scheme of formamide are given as follows:

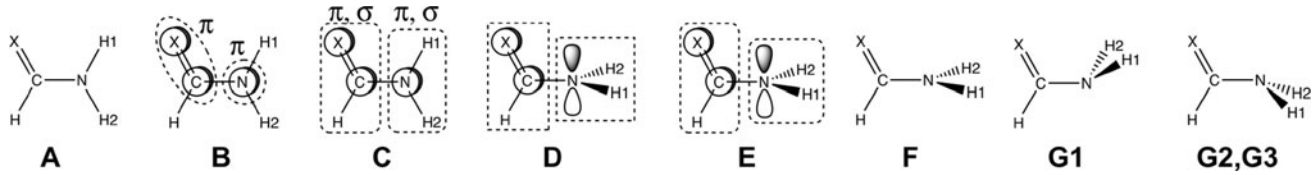

[a] The geometry is derived from a 180° rotation of the amino group around the C–N bond in structure **G1**

$$\Psi^{\mathbf{C}}_{\mathrm{SRHF}} = \hat{A}\left(\Phi^{\mathbf{C}}_{\sigma}\Phi^{\mathbf{C}}_{\mathrm{CHO}}\Phi^{\mathbf{C}}_{\mathrm{NH_2}}\right), \tag{35}$$

in which the symbol σ of $\Phi^{\mathbf{C}}_{\sigma}$ denotes the remaining σ orbitals, $1s_C$, $1s_N$, $1s_O$, and σ_{CN} orbitals in the SRHF state; $\Phi^{\mathbf{C}}_{\mathrm{CHO}} = \varphi^{\mathbf{C}}_{\pi_{CO}}\bar{\varphi}^{\mathbf{C}}_{\pi_{CO}}\varphi^{\mathbf{C}}_{\sigma_{CO}}\bar{\varphi}^{\mathbf{C}}_{\sigma_{CO}}\varphi^{\mathbf{C}}_{\sigma_{CH}}\bar{\varphi}^{\mathbf{C}}_{\sigma_{CH}}\varphi^{\mathbf{C}}_{n_{\sigma O}}\bar{\varphi}^{\mathbf{C}}_{n_{\sigma O}}\varphi^{\mathbf{C}}_{n_{\pi O}}\bar{\varphi}^{\mathbf{C}}_{n_{\pi O}}$, where $n_{\sigma O}$ and $n_{\pi O}$ indicate the O lone pairs along and perpendicular to the C–O axis, respectively; and $\Phi^{\mathbf{C}}_{\mathrm{NH_2}} = \varphi^{\mathbf{C}}_{n_N}\bar{\varphi}^{\mathbf{C}}_{n_N}\varphi^{\mathbf{C}}_{\sigma_{NH1}}\bar{\varphi}^{\mathbf{C}}_{\sigma_{NH1}}\varphi^{\mathbf{C}}_{\sigma_{NH2}}\bar{\varphi}^{\mathbf{C}}_{\sigma_{NH2}}$.

Then, by a 90° rotation about the C–N *single* bond in this structure with the remaining structural parameters unchanged, the 90°-twisted structure (structure **D**) is obtained. The SRHF state of structure **D** without any relaxation of the SRMOs in structure **C** is expressed as

$$\Psi^{\mathbf{D}'}_{\mathrm{SRHF}} = \hat{A}\left(\Phi^{\mathbf{D}'}_{\sigma}\Phi^{\mathbf{C}}_{\mathrm{CHO}}\Phi^{\mathbf{C}}_{\mathrm{NH_2}}\right), \tag{36}$$

where $\mathbf{D}'$ indicates that the SRMOs are not relaxed in structure **D**, and $\Phi^{\mathbf{D}'}_{\sigma}$ is generated by simply rotating the amino group part of $\Phi^{\mathbf{C}}_{\sigma}$ by 90°. Although $\Psi^{\mathbf{D}'}_{\mathrm{SRHF}}$ can represent the state where the in-plane and out-of-plane CT interactions between two groups are properly deactivated, this state is obviously far from the *minimum-energy* SRHF state in this structure:

$$\Psi^{\mathbf{D}}_{\mathrm{SRHF}} = \hat{A}\left(\Phi^{\mathbf{D}}_{\sigma}\Phi^{\mathbf{D}}_{\mathrm{CHO}}\Phi^{\mathbf{D}}_{\mathrm{NH_2}}\right). \tag{37}$$

Figure 3 gives the DED map between the unrelaxed and relaxed n_N orbitals in structure **D**, that is, $\varphi^{\mathbf{C}}_{n_N}$ and $\varphi^{\mathbf{D}}_{n_N}$, and this map shows that during relaxation, this lone pair shrinks to reduce the overlap repulsion. This $\Psi^{\mathbf{D}}_{\mathrm{SRHF}}$ properly takes the electrostatic environment into account and further maintains the deactivation of the interactions in succession to $\Psi^{\mathbf{D}'}_{\mathrm{SRHF}}$.

Clearly, structure **D** is different from the structure optimized at the SRHF/6-31G(d) level under the constraint by which the planar amino group is perpendicular to the planar formyl group (structure **E**). Structure **E** with C_s symmetry is the most stable 90°-twisted structure when the intramolecular CT interactions between the formyl and planar amino groups are deactivated. The SRHF state in this structure is represented as

$$\Psi^{\mathbf{E}}_{\mathrm{SRHF}} = \hat{A}\left(\Phi^{\mathbf{E}}_{\sigma}\Phi^{\mathbf{E}}_{\mathrm{CHO}}\Phi^{\mathbf{E}}_{\mathrm{NH_2}}\right). \tag{38}$$

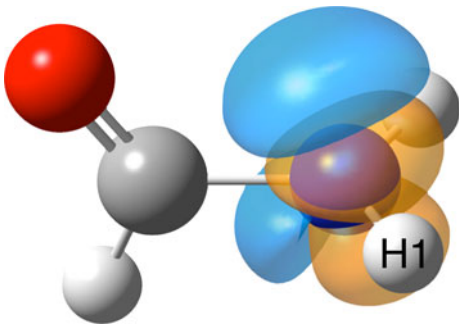

Fig. 3 DED map for the 90°-rotated conformation of formamide (structure **D**) that represents the change of the nitrogen lone pair to reduce the overlap repulsions related to this lone pair. The coloring scheme for the surface is the same as in Fig. 2, and the isosurface values are 0.0002 *e*/bohr^3

when structure **C** changes to structure **E**, the C–N bond length increases by 0.035 Å, and the ∠O–C–H bond angle decreases by 1.5° owing to the Pauli repulsion (Table 1). These small variations in the geometry originate from the fact that structure **C** successfully represents the structure with the *localized* electronic state.

Now, let us partition the total CT interaction in structure **E** into various in-plane and out-of-plane CT interactions in terms of energy. The interaction energy components attributable to these CT interactions were obtained by subtracting the energy of the SRHF state with only a target interaction deactivated from that of the HF state. Furthermore, an energy component was decomposed into some subcomponents through proper selection of the deactivated interaction (see Appendix 3 for the detailed derivation of energy subcomponents). The results are given in Table 2, in which the results of using several other basis sets [77–79] are also listed to explore the basis set dependence of the interaction energy and the energy components according to the SRW approach. The electron delocalization occurs from the amino group to the formyl group more easily than from the formyl group to the amino group, in accord with the electronegativity of the O atom. Subcomponents are almost additive in every component except those with the strong coupling between them. For instance, the total CT interaction energy (−11.69 kcal/mol) is nearly equal to the sum of $E(\mathrm{NH_2} \rightarrow \mathrm{CHO})$ (−8.84 kcal/mol) and $E(\mathrm{CHO} \rightarrow \mathrm{NH_2})$ (−2.95 kcal/mol), whereas $E\left(\mathrm{n_N} \rightarrow \sigma^*_{\mathrm{CH+CO}}\right)$ (−5.63 kcal/mol) is considerably smaller than the sum of $E\left(\mathrm{n_N} \rightarrow \sigma^*_{\mathrm{CH}}\right)$ (−4.24 kcal/mol) and $E\left(\mathrm{n_N} \rightarrow \sigma^*_{\mathrm{CO}}\right)$ (−3.96 kcal/mol), indicating the strong coupling in this case. Focusing on each energy component, we found that the negative hyperconjugation (e.g., $\mathrm{n_N} \rightarrow \sigma^*_{\mathrm{CH}}$ interaction) exerts a stronger influence on the stability of structure **E** than does the hyperconjugation (e.g., $\pi_{\mathrm{2NH}} \rightarrow \pi^*_{\mathrm{CO}}$ interaction). This is consistent with chemical intuition, according to which lone-pair electrons are more mobile than bonding electrons. In addition, Table 2 exhibits the small basis set dependence of the interaction energy and energy components determined by the SRW method in the moderately large basis sets.

The results in Table 2 are energy changes in structure **E**, and in fact, the CT interactions activated in structure **E** lead to another structure. Structure **F** resulting from these interactions is the twisted HF structure with C_s symmetry, which keeps the amino group planar. In changing from structure **E** to structure **F**, the C–N bond length decreases by 0.058 Å, whereas the remaining bond lengths increase somewhat (Table 1). This structure change is consistent with the theoretical predictions. The HF state of structure **F** is expressed as

$$\Psi^{\mathbf{F}}_{\mathrm{HF}} = \hat{A}\left(\Phi^{\mathbf{F}}_{\sigma_{\mathrm{HF}}}\Phi^{\mathbf{F}}_{\mathrm{HF(CHO)}}\Phi^{\mathbf{F}}_{\mathrm{HF(NH_2)}}\right), \tag{39}$$

where $\Phi^{\mathbf{F}}_{\mathrm{HF(CHO)}} = \phi^{\mathbf{F}}_{\pi_{\mathrm{CO}}}\bar{\phi}^{\mathbf{F}}_{\pi_{\mathrm{CO}}}\phi^{\mathbf{F}}_{\sigma_{\mathrm{CO}}}\bar{\phi}^{\mathbf{F}}_{\sigma_{\mathrm{CO}}}\phi^{\mathbf{F}}_{\sigma_{\mathrm{CH}}}\bar{\phi}^{\mathbf{F}}_{\sigma_{\mathrm{CH}}}\phi^{\mathbf{F}}_{\mathrm{n}_{\sigma\mathrm{O}}}\bar{\phi}^{\mathbf{F}}_{\mathrm{n}_{\sigma\mathrm{O}}}\phi^{\mathbf{F}}_{\mathrm{n}_{\pi\mathrm{O}}}\bar{\phi}^{\mathbf{F}}_{\mathrm{n}_{\pi\mathrm{O}}}$ and $\Phi^{\mathbf{F}}_{\mathrm{HF(NH_2)}} = \phi^{\mathbf{F}}_{\mathrm{n_N}}\bar{\phi}^{\mathbf{F}}_{\mathrm{n_N}}\phi^{\mathbf{F}}_{\sigma_{\mathrm{NH1}}}\bar{\phi}^{\mathbf{F}}_{\sigma_{\mathrm{NH1}}}\phi^{\mathbf{F}}_{\sigma_{\mathrm{NH2}}}\bar{\phi}^{\mathbf{F}}_{\sigma_{\mathrm{NH2}}}$. Finally, by allowing the amino N atom to pyramidalize, the two transition-state structures of C_s symmetry for the amino group rotation are obtained. Then, the conformers with the N lone pair being anti and syn to the carbonyl group are called structures **G1** and **G2**, respectively, and the HF state of the former is more stable than that of the latter by 2.86 kcal/mol:

$$\Psi^{\mathbf{Gi}}_{\mathrm{HF}} = \hat{A}\left(\Phi^{\mathbf{Gi}}_{\sigma_{\mathrm{HF}}}\Phi^{\mathbf{Gi}}_{\mathrm{HF(CHO)}}\Phi^{\mathbf{Gi}}_{\mathrm{HF(NH_2)}}\right) \quad (\mathbf{i} = \mathbf{1}, \mathbf{2}). \tag{40}$$

To examine this energy difference, EDA using the SRW method was performed for structures **G1** and **G3.** The latter, in place of structure **G2**, is generated by a 180° rotation of the amino group around the C–N bond in structure **G1** (see Table 1). Structure **G3** is used because if the subspaces in structure **G3** are isolated (the SIHF state), E_{SIHF} in structure **G3** is identical to that in structure **G1**, and this facilitates direct comparison in the components between the conformers. In this analysis, the initial occupied and virtual SRMOs were used instead of the SIMOs in the SRW decomposition scheme; the SRW calculations gave the following electrostatic states with the three subspaces:

$$\Psi^{\mathbf{Gi}}_{\mathrm{SRHP}} = \hat{A}\left(\Phi^{\mathbf{0Gi}}_{\sigma}\right)\hat{A}\left(\Phi^{\mathbf{0Gi}}_{\mathrm{CHO}}\right)\hat{A}\left(\Phi^{\mathbf{0Gi}}_{\mathrm{NH_2}}\right) \quad (\mathbf{i} = \mathbf{1}, \mathbf{3}) \tag{41}$$

and

$$\Psi^{\mathbf{Gi}}_{\mathrm{SRHF}} = \hat{A}\left(\Phi^{\mathbf{Gi}}_{\sigma}\Phi^{\mathbf{Gi}}_{\mathrm{CHO}}\Phi^{\mathbf{Gi}}_{\mathrm{NH_2}}\right) \quad (\mathbf{i} = \mathbf{1}, \mathbf{3}). \tag{42}$$

Although the results thus obtained are not quite as good as those using the SIMOs, as mentioned in Sect. 2.3.1, the analysis with the initial SRMOs would work well when electronic structures of the subspaces in one conformer

Table 2 Energy decomposition of the total CT interaction between the formyl and planar amino groups in the 90°-twisted structure of formamide optimized at the SRHF/6-31G(d) level (structure **E**)

Interaction	Basis Set		
	6-31G(d)	6-31+G(d,p)	6-311G(d,p)
Total CT interaction	−11.69	−12.22	−12.37
· $NH_2 \rightarrow CHO$	−8.84	−9.64	−9.34
·$n_N \rightarrow \sigma^*_{CH+CO}$	−5.63	−6.07	−5.79
▪$n_N \rightarrow \sigma^*_{CH}$	−4.24	−4.19	−4.48
▪$n_N \rightarrow \sigma^*_{CO}$	−3.96	−3.79	−3.70
·$(\sigma_{2NH}+\pi_{2NH}) \rightarrow (\sigma^*_{CH+CO}+\pi^*_{CO}+2p^*_C)$ [a]	−3.10	−3.47	−3.43
▪$(\sigma_{2NH}+\pi_{2NH}) \rightarrow (\sigma^*_{CO}+\pi^*_{CO})$	−3.06	−3.39	−3.35
·$\sigma_{2NH} \rightarrow \sigma^*_{CO}$	−0.28	−0.45	−0.33
·$\pi_{2NH} \rightarrow \pi^*_{CO}$	−2.76	−2.92	−3.01
▪$(\sigma_{2NH}+\pi_{2NH}) \rightarrow (\sigma^*_{CH}+2p^*_C)$ [a]	−1.27	−1.41	−1.46
·$\sigma_{2NH} \rightarrow \sigma^*_{CH}$	−0.29	−0.47	−0.36
·$\pi_{2NH} \rightarrow 2p^*_C$ [a]	−0.99	−0.95	−1.10
· $CHO \rightarrow NH_2$	−2.95	−2.66	−3.13
·$(\sigma_{CO}+\pi_{CO}+n_{\sigma O+\pi O}) \rightarrow (\sigma^*_{2NH}+\pi^*_{2NH})$	−2.00	−1.84	−2.32
▪$\sigma_{CO} \rightarrow \sigma^*_{2NH}$	−0.18	−0.22	−0.18
▪$\pi_{CO} \rightarrow \pi^*_{2NH}$	−0.98	−1.08	−1.18
▪$n_{\sigma O+\pi O} \rightarrow \sigma^*_{2NH}$	−0.86	−0.57	−0.98
·$n_{\sigma O} \rightarrow \sigma^*_{2NH}$	−0.07	−0.08	−0.06
·$n_{\pi O} \rightarrow \sigma^*_{2NH}$	−0.79	−0.48	−0.92
·$\sigma_{CH} \rightarrow \sigma^*_{2NH}$	−1.05	−0.89	−0.91

All values are in kcal/mol

σ_{2NH} and π_{2NH} denote the orbitals resulting from the symmetric and antisymmetric combinations of the two σ_{NH} orbitals (*symmetry-adapted* linear combination), respectively, and their antibonding counterparts are expressed as σ^*_{2NH} and π^*_{2NH}

$2p^*_C$ and $2p^*_N$ stand for the 2p orbitals on the C and N atoms of π^*_{CO} and σ^*_{CN}, respectively

Typical notations are employed to express the electron-accepting orbitals. Depending on the energy levels of electron-accepting orbitals and the overlap between the electron-donating and -accepting orbitals, an alternative orbital could accept electron density from the electron-donating orbital. For example, in the $\sigma_{CH} \rightarrow \sigma^*_{2NH}$ interaction, there would be some accepting orbitals, such as σ^*_{2NH}, $3p_N$, and $2p^*_N$

[a] With the 6-31+G(d,p) and 6-311G(d,p) basis sets, $2p_H$ is included in the electron-accepting orbitals

(structure **G1**) resemble those in another conformer (structure **G3**). This is because errors associated with the use of the initial SRMOs are effectively canceled out, focusing on the difference between these conformers. In addition, the difference in E_{ES} between two conformers, ΔE_{ES}, is calculated from the difference in other energy components:

$$\Delta E_{ES} = \Delta E_{INT} - \Delta E_{EE} - \Delta E_{Pauli} - \Delta E_{POL} - \Delta E_{CT}. \quad (43)$$

The results of the EDA are summarized in Table 3, together with those of the KM analysis carried out using the GAMESS package [80]. The isolated fragments in the KM analysis were assumed to be CHO^+ cation and NH_2^- anion. According to the EDA based on our SRW method, the energy components in structure **G3** indicate that the destabilization due to the Pauli repulsion cannot be compensated for by other favorable interactions. In the KM analysis, the EX interaction causes structure **G3** to be destabilized, and furthermore, the CT and ES interactions do not lead to the stabilization of this structure as compared to structure **G1**. As a result, in both the analyses, the anti rotamer (structure **G1**) is relatively stable owing to the larger repulsion in the syn rotamer (structure **G3**). Therefore, the SRW method gives the results along the well-known KM method, and meanwhile, it is expected to provide another perspective on the behavior of electrons in intramolecular interaction owing to the different definition and meaning of the energy components from the KM method [1].

Table 3 Energy decomposition analysis in the transition-state structures for the amino group rotation in formamide (structures **G1** and **G3**) by the use of our space-restricted wave function (SRW) method and the Kitaura–Morokuma (KM) method with the 6-31G(d) basis set

Method	ES	EE EX	Pauli	POL[a] PL	CT	MIX	INT
SRW	−5.55	−7.83	17.98	−0.52	−0.85	–	3.23
KM	2.94	5.40	–	−0.90	5.85	−0.65	12.64

The differences in energy component relative to structure **G1**

All values are in kcal/mol

[a] The polarization interaction in the SRW method is calculated in the presence of the EX interaction, differently from the KM method

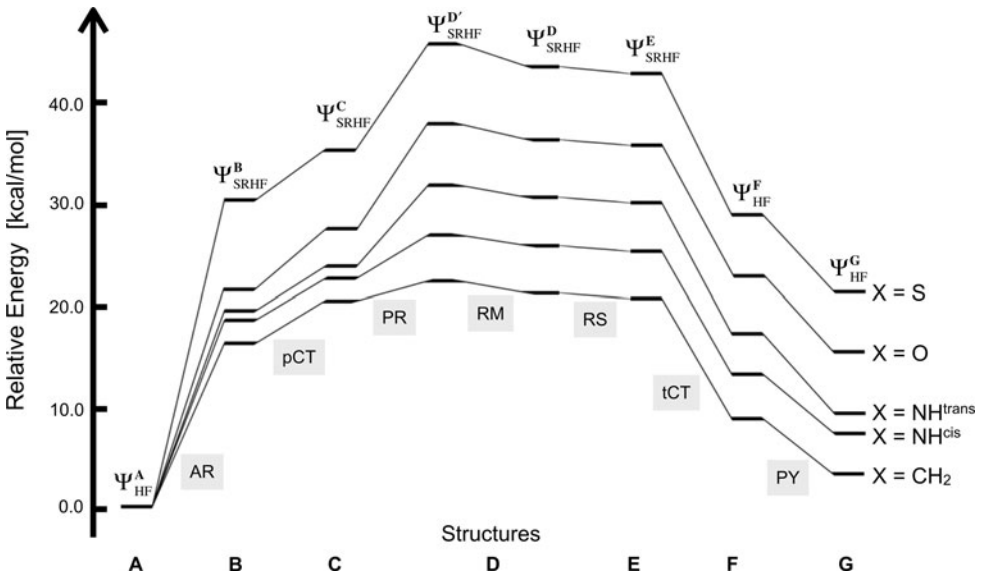

Fig. 4 Schematic diagram of the energy contributions to the rotational barrier of the amino group around the C–N bond in formamide and its analogous molecules, HC(=X)NH_2 (see text for details). The structures indicated by **A** to **G** are given in the footnote of Table 1. For clarity in this figure, the more stable state of the two transition-state structures for the amino group rotation (structure **G1** or **G2**) is shown as structure **G**

The results of the investigation of the internal rotational barrier in formamide using the energies in structures **A** to **G** thus obtained are summarized schematically in Fig. 4. This figure indicates the decomposition of this barrier into seven components, each of which is calculated as the energy difference between two adjacent structures. Each component corresponds to the characteristic effect as follows: (1) adiabatic resonance effect (AR), (2) in-plane CT effect in the planar conformation (pCT), (3) *pure* rotation (PR), (4) relaxation of the SRMOs (RM), (5) relaxation of the geometric structure (RS), (6) in-plane/out-of-plane CT effect in the twisted conformation (tCT), and (7) pyramidalization (PY); these energy values are listed in Table 4. The energy components attributable to AR and pCT were calculated as the energy change upon the loss of these components, whereas the other components were the energy changes resulting from the corresponding effects.

Figure 4 shows that the sum of the energies contributing to the stabilization of structure **G** (RM, RS, tCT, and PY) cannot compensate for the energies resulting in the destabilization of this structure (AR, pCT, and PR). The main effects responsible for destabilizing the structure are AR and PR (see X=O in Fig. 4 and Table 4), and the latter is caused mainly by the $\sigma_{CH} - n_N$, $\sigma_{CO} - n_N$, and $n_{\pi O} - n_N$ overlap repulsions owing to their large overlap in the 90°-twisted structure rotated around the C–N bond from the planar structure. Consequently, the rotational barrier of the amino group in formamide is attributed to both the loss of the resonance interaction and the increase in the repulsive interaction.

In addition, the results of an analysis of the rotational barrier in the isoelectronic chalcogen analogs, HC(=X)NH_2 (X=CH_2, NH^{cis}, NH^{trans}, and S), are presented in Table 4 and Fig. 4, where NH^{cis} and NH^{trans} denote the imino hydrogens oriented cis and trans to the amino group, respectively (the structural parameters of these analogs are tabulated in Table S1–S4). The energy components of the internal rotation barrier in all analogs show that while the signs of the components are the same as those of formamide, their values are not similar, especially in E_{AR}, E_{PR}, and E_{PY}. To examine the characteristics of the analogs, these three energy components are discussed in detail below. For ease of comparison, we employed the planar structures (structure **A**) as the ground-state structures for

Table 4 Energy contributions to the total barrier of the rotation of the amino group around the C–N bond in formamide and its analogous molecules, HC(=X)NH_2 (X=O, CH_2, NH^{cis}, NH^{trans}, and S)

X	Energy component [kcal/mol]								
	AR	pCT	PR	RM	RS	tCT	PY[a]		Total barrier
							1	2	
O	22.48	5.06	10.55	−1.58	−0.46	−13.13	−7.24	−4.38	15.69
CH_2	16.74	4.04	2.32	−1.38	−0.30	−12.67	−4.26	−5.53	3.22
NH^{cis}	18.57	4.61	4.62	−1.44	−0.45	−12.58	−3.72	−5.93	7.39
NH^{trans}	19.77	4.77	7.36	−1.60	−0.33	−13.66	−7.04	−4.01	9.26
S	30.30	5.59	10.60	−2.07	−0.56	−15.32	−7.14	−4.78	21.38

[a] PY1 and PY2 were given with structures **G1** and **G2**, respectively

vinylamine and both formamidine conformers, despite the fact that they have a pyramidal amino group.

E_{AR} becomes larger as the electronegativity of the atom double-bonded to the central C atom increases, except with thioformamide. A similar trend is observed in other types of CT interaction: E_{pCT} and E_{tCT}. Wiberg et al. have shown that π-electron charge transfer from N to C is a dominant factor for the rotational barrier in formamide, and the polarization in the C=O bond described by the resonance between Lewis structures I and II is important [49]. The larger electronegativity of the atom double-bonded to the central C atom would make the central C atom more electron-accepting. This results in larger participation of Lewis structure III and thus a larger rotational barrier. In addition, Wiberg et al. have reported the following: because of the small difference in electronegativity between the C and S atoms, the C=S bond is not as polarized as the C=O bond in formamide, making the C atom in thioformamide a poor electron acceptor; nevertheless, because of its larger size, the S atom can accept the electrons [53]. Consequently, Wiberg et al. suggested that thioformamide is best described by the resonance between I and III (X=S). To verify this suggestion, AR was further analyzed using the MO-pair analysis technique as well as the SRW method; these results are shown in Fig. 5. The DED-LB map (Fig. 5a) accurately indicates that upon the CT interaction, the lone-pair electrons on the N atom in thioformamide delocalize over the C and S atoms more than those in vinylamine do over the corresponding atoms (Fig. 5c). The shape and size of the lobe on the central C atom in thioformamide are similar to those in formamide (see Fig. 2a). Thus, it can be stated that regardless of the small difference in electronegativity, the π^*_{CS} orbital is polarized toward this C atom to a similar extent as the π^*_{CO} orbital.

Let us now focus on the electron affinity of the O, C, and S atoms, the magnitudes of which follow the order C < O < S. Then, in addition to $\Psi^{\mathbf{A}}_{SRHF}$, we calculate two SRHF states: $\Psi^{\mathbf{A}}_{SRHF_1} = \hat{A}\left(\Phi^{\mathbf{A}}_{\sigma}\varphi^{\mathbf{A}}_{\pi_{CN}}\varphi^{\mathbf{A}}_{n_X}\right)$ and $\Psi^{\mathbf{A}}_{SRHF_2} = \hat{A}\left(\Phi^{\mathbf{A}}_{\sigma}\varphi^{\mathbf{A}}_{n_X}\varphi^{\mathbf{A}}_{n_N}\right)$, in which n_X denotes the C, O, or S lone

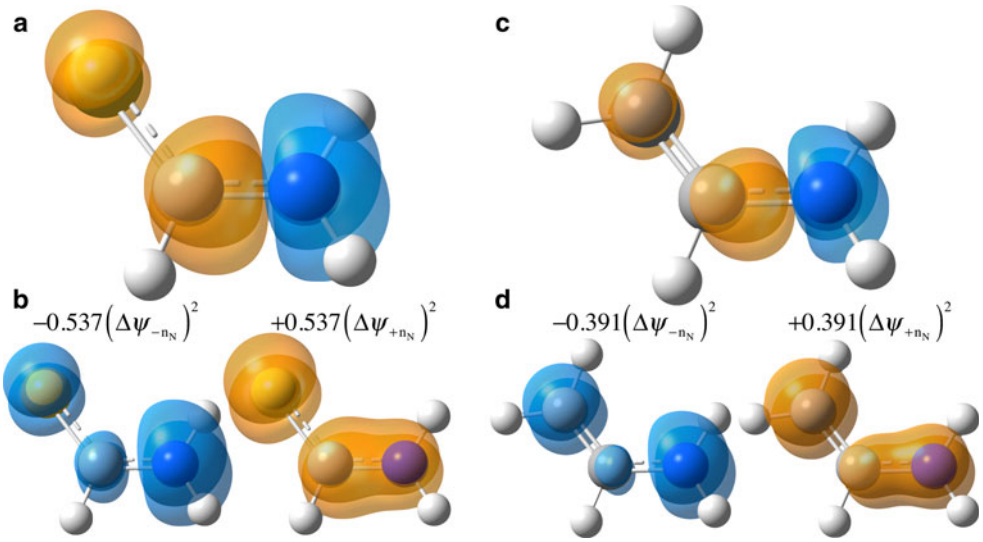

Fig. 5 **a** DED-LB map for the $n_N \rightarrow \pi^*_{CS}$ interaction and **b** the weighted densities of the complementary DDNOs obtained from the DED-LB in the planar HF structure (structure **A**) of thioformamide. **c** DED-LB map for the $n_N \rightarrow \pi^*_{CC}$ interaction and **d** the weighted densities of the complementary DDNOs from the DED-LB in the planar HF structure (structure **A**) of vinylamine. The coloring scheme for the surface and the isosurface values are the same as in Fig. 2

Table 5 Three SRHF states in formamide, vinylamine, and thioformamide in structure **A** together with the C–N bond lengths and atomic charges on the N atom in their HF states

	X		
	O	CH_2	S
State	SRHF energy		
SRHF[a]	−168.89007	−133.028735	−491.509708
$SRHF_1$[b]	44.76	76.70	7.47
$SRHF_2$[b]	79.94	106.56	54.32
	C–N bond length [Å]		
	1.348	1.371	1.324
	Natural charge on the N Atom [*e*]		
	−0.926	−0.907	−0.843

[a] Values are in hartree

[b] Values are relative to the SRHF state and are in kcal/mol (see text)

pair orbital. $\Psi^{\mathbf{A}}_{SRHF_1}$ represents Lewis structure III and also involves the polarization in the C–N π bond described by Lewis structure II, and $\Psi^{\mathbf{A}}_{SRHF_2}$ corresponds to Lewis structure II. Table 5 gives the energies of $SRHF_1$ and $SRHF_2$ states relative to the SRHF state, the order of which correlates well with the electron affinities of the C, O, and S atoms. These results clearly show that the $SRHF_1$ state in thioformamide can contribute significantly to the resonance effect, whereas that in vinylamine and in formamide does not. In other words, in thioformamide, the importance of the $SRHF_1$ state for the HF state would be comparable to that of the SRHF state, whereas the $SRHF_2$ state is less important if the HF state is represented by the superposition of the SRHF, $SRHF_1$, and $SRHF_2$ states. This is evidenced by the shortest C–N bond length as well as the most positive N atomic charge in their HF states (see Table 5) [81, 82][4]. Furthermore, this charge difference is consistent with the results indicating that the number of electrons that are allowed to flow from the N lone pair is larger in thioformamide than in formamide and vinylamine (see Figs. 2b, 5b, d). We conclude that the large electron affinity of the S atom enhances the importance of the covalent character of the π bond between the C and N atoms, which is included only in the $SRHF_1$ state, and this leads to the strong resonance effect in thioformamide.

The destabilization energy from the pure rotation (E_{PR}) increases in the same order as the overlap between the amino N lone pair and its nearest bonding orbital (X=CH_2 and NH^{cis}), or the lone pair (X=O, NH^{trans}, and S) in the substituents increases in $\Psi^{\mathbf{D}'}_{SRHF}$: vinylamine (0.0353) < formamidines (0.0393) < formamide (0.0565) < thioformamide (0.0635). The difference between cis and trans formamidines arises mainly from the larger overlap repulsion between the amino N lone pair and the C=N σ_{CN} bond in the trans conformer, which has the smaller ∠N–C–N bond angle (see Table S2 and S3). For pyramidalization (E_{PY}), the results observed in vinylamine and cis formamidine are opposite to the result observed in formamide; this was explained using the EDA results for structures **G1** and **G3**. In other words, in these two analogs, the structural change from structure **F** to **G2** is more stabilized than that from structure **F** to **G1**. This is probably because in the syn rotamer of the analogs, the stabilization resulting from intramolecular hydrogen bonding between the amino N lone pair and the H atom in each substituent is larger than the destabilization originating from Pauli repulsion between the lone pair and substituent.

Finally, it should be noted that structures **C**, **D**, and **E** cannot be produced by the BLW method. This is because the different subsets describing the subspaces must share the same basis functions to produce these structures.[5] For instance, in structure **E** of formamide, while $\varphi_{\sigma_{CN}}$ and φ_{n_N} are expanded in the different subspaces, the basis functions on the N atom describing these SRMOs of σ symmetry need to be shared, and this situation requires that the type 2 and 3 subspaces are employed. Let us consider the 90°-twisted structure with the planar amino group optimized by the BLW method from structure **B**. This structure clearly corresponds to structure **E** and thus is called structure $\mathbf{E_B}$. The BLW state of structure $\mathbf{E_B}$ does not reflect the electronic and conformational effects in this structure for the reason mentioned above, though the BLW state of the planar structure is fully relaxed. Consequently, we can conclude that the BLW method would often provide the upper limit of the energy of the "electron-localized" state, such as the electronic state in structure **E**. Taking as an example the analysis of in-plane/out-of-plane CT interactions in the twisted conformation (tCT) of formamide, the calculated $\pi_{2NH} \rightarrow \pi^*_{CO}$ and $n_N \rightarrow \sigma^*_{CO}$ interaction energies in structure **E** according to the SRW approach are −2.76 and −3.96 kcal/mol, respectively; those in structure $\mathbf{E_B}$ according to the BLW method are −4.9 and −8.1 kcal/mol, respectively [32]. These energetic relationships indicate that the SRHF state can adequately represent the fully relaxed electronic state without the CT interactions between the formyl and amino groups.

4 Concluding remarks

We have developed a new approach that can yield the electronic states with various types of intramolecular

[4] Supplementary calculations were performed to ensure the qualitative accuracy of our results (see Supporting Information for details).

[5] The basis functions we mentioned here were derived from the symmetry-adapted linear combination of the functions in the selected basis set.

interaction deactivated for the purpose of analyzing the interaction, without breaking bonds in a molecule. By employing these states as the zeroth-order wave functions in the EDA scheme, the total interaction energy can be decomposed into various energy components, each of which gives chemical characteristics of the electronic behavior. In relation to eliminating the restriction in the well-known methods of analyzing the interaction, there are three important points in our SRW method:

1. The initial occupied SRMOs are generated from the NLMOs to facilitate the estimation of the orbital characters. This enables us to view the SRMO and its parent NLMO as a pair and then perform an MO-pair analysis.
2. The subspace to which electrons are confined is classified into three types based on the relation to another subspace. The variational spaces in the type 2 and 3 subspaces are reduced to avoid unexpected changes in the occupied part of the subspaces.
3. In our SCF procedure, every occupied SRMO in a subspace is updated through one SCF cycle, and the order of updating the subspaces follows that of increasing number of basis functions describing a subspace. This condition is required in order to promote a dramatic change in the SRMO from its parent NLMO.

In the present work, we first applied the SRW method to the analysis of the resonance and the rotational barrier in formamide, vinylamine, formamidine, and thioformamide. In the planar conformation of formamide, the electronic state without the CT interaction of the N lone pair is properly represented by the SRHF state, and for further investigation, the MO-pair analysis technique using the DED-LB map with the complementary DDNOs was proposed. Then, to clarify the energy contribution to the barrier in the amino group rotation around the C–N bond, seven structures were generated by the geometry optimization at the SRHF/6-31G(d) and HF/6-31G(d) levels (structures **A** to **C**, **E**, **F**, **G1**, and **G2**). Among these, structures **C** and **E** were obtained under the condition that the CT interactions between formyl or its analogous group and the amino group are deactivated. The energy differences between two successive structures show that the rotational barrier of the amino group rotation originates mainly from the disappearance of the resonance and the enlargement of the repulsion.

In structure **E** of formamide, the energy differences between the HF and SRHF states—that is, interaction energies of the in-plane/out-of-plane CT interactions—exhibit the small basis set dependence. Furthermore, through comparison with the results of the BLW method, it was confirmed that the SRHF state can accurately represent the fully relaxed electronic state, taking into account the electrostatic environment of the system with these interactions eliminated. To determine the main factor for the energy difference between the transition-state structures for the amino group rotation (structures **G1** and **G2**) in formamide, EDA with the SRW method was carried out. This analysis revealed that the Pauli repulsion makes structure **G1** more stable than structure **G2**. In addition, the adiabatic resonance effect in thioformamide is stronger than in formamide and vinylamine; based on the results for the SRHF energy as well as the MO-pair analysis technique, we attribute this to the large electron affinity of the S atom.

We have shown the applicability of our SRW approach, and based on the analyses, we have confirmed that this approach can successfully and stably produce the fully relaxed electronic state without various types of intramolecular interaction. We expect that the SRW method will prove helpful in understanding the interactions, even those that seem complicated, in a system. Further studies, including development of this method in the framework of DF theory and investigation of the details of the SIHF state, are in progress.

Acknowledgments This research was supported by the Core Research for Evolutional Science and Technology (CREST) "High Performance Computing for Multi-scale and Multi-physics Phenomena" from the Japan Science and Technology Agency. Some of the calculations were carried out at the research center for computational science, Okazaki, Japan.

Appendix 1: Initial occupied *k*-SRMOs

In accordance with the assumption of the space as mentioned at the beginning of Sect. 2.1, the NLMOs (Eq. 10) are classified into K groups, each of which has n_{o}^{k} NLMOs:

$$\begin{aligned}\boldsymbol{\phi}^{k} &= \begin{pmatrix} \phi_1^k & \cdots & \phi_i^k & \cdots & \phi_{n_{\mathrm{o}}^k}^k \end{pmatrix} \\ &= \boldsymbol{\chi}\mathbf{L}^{k}.\end{aligned} \tag{44}$$

The tentative initial occupied k-SRMOs are generated by deleting the unused space $\Delta_{\mathrm{tails}}^{k}$ from the NLMOs belonging to the kth group:

$$\begin{aligned}\tilde{\boldsymbol{\varphi}}_{\mathrm{o}}^{0,k} &= \boldsymbol{\chi}\mathbf{R}_{\mathrm{tails}}^{k}\mathbf{L}^{k} \\ &= \boldsymbol{\chi}\tilde{\mathbf{T}}^{0,k},\end{aligned} \tag{45}$$

in which $\mathbf{R}_{\mathrm{tails}}^{k}$ is the diagonal matrix with either a zero or a one for the νth diagonal element, which corresponds to whether or not the νth basis function is used to describe $\Delta_{\mathrm{tails}}^{k}$. Then, these tentative initial occupied k-SRMOs become the initial occupied k-SRMOs by the symmetric orthogonalization:

$$\begin{aligned}\boldsymbol{\varphi}_{\mathrm{o}}^{0,k} &= \left(\varphi_1^{0,k} \quad \cdots \quad \varphi_i^{0,k} \quad \cdots \quad \varphi_{n_{\mathrm{o}}^k}^{0,k}\right) \\ &= \boldsymbol{\chi}\tilde{\mathbf{T}}^{0,k}\left(\tilde{\mathbf{T}}^{0,k+}\mathbf{S}\tilde{\mathbf{T}}^{0,k}\right)^{-\frac{1}{2}} \\ &= \boldsymbol{\chi}\mathbf{T}^{0,k}.\end{aligned} \tag{46}$$

Appendix 2: Pseudo-occupied *k*-SRMOs

In the type 3 *k*th subspace, the pseudo-occupied *k*-SRMOs, $\boldsymbol{\varphi}_{\mathrm{p}}^{0,k}$, are prepared from the occupied SRMOs of every k'th subspace ($k' = k_1$, k_2, and k_3, for example), as follows:

1. $\boldsymbol{\varphi}_{\mathrm{o}}^{0,(k)}$ is defined with all initial occupied SRMOs of the corresponding subspaces:

$$\begin{aligned}\boldsymbol{\varphi}_{\mathrm{o}}^{0,(k)} &= \left(\boldsymbol{\varphi}_{\mathrm{o}}^{0,k_1} \quad \boldsymbol{\varphi}_{\mathrm{o}}^{0,k_2} \quad \boldsymbol{\varphi}_{\mathrm{o}}^{0,k_3}\right) \\ &= \boldsymbol{\chi}\mathbf{T}^{0,(k)}.\end{aligned} \tag{47}$$

2. Of $\boldsymbol{\varphi}_{\mathrm{o}}^{0,(k)}$ treated with $\mathbf{R}_{\mathrm{tails}}^k$ (Eq. 45), the candidates for the pseudo-occupied *k*-SRMOs are chosen in accordance with the norm:

$$\begin{aligned}\tilde{\boldsymbol{\varphi}}_{\tilde{\mathrm{p}}}^{0,k} &= choice\left(\boldsymbol{\chi}\mathbf{R}_{\mathrm{tails}}^k\mathbf{T}^{0,(k)}\right) \\ &= \boldsymbol{\chi}\tilde{\mathbf{T}}_{\tilde{\mathrm{p}}}^{0,k},\end{aligned} \tag{48}$$

where $choice(\boldsymbol{\varphi})$ is the operator that removes from $\boldsymbol{\varphi}$ the column vectors having norms smaller than the threshold value, presently set to 0.6.

3. By the Gram–Schmidt orthogonalization to the *actual* occupied *k*-SRMOs ($\boldsymbol{\varphi}_{\mathrm{o}}^{0,k}$), $\tilde{\boldsymbol{\varphi}}_{\mathrm{p}}^{0,k}$ is generated from the candidates according to Eq. 49:

$$\begin{aligned}\tilde{\boldsymbol{\varphi}}_{\mathrm{p}}^{0,k} &= \boldsymbol{\chi}\left(\mathbf{1} - \mathbf{T}^{0,k}\mathbf{T}^{0,k+}\mathbf{S}\right)\tilde{\mathbf{T}}_{\tilde{\mathrm{p}}}^{0,k} \\ &= \boldsymbol{\chi}\tilde{\mathbf{T}}_{\mathrm{p}}^{0,k}\end{aligned}. \tag{49}$$

4. The Gram–Schmidt orthonormalization of $\tilde{\boldsymbol{\varphi}}_{\mathrm{p}}^{0,k}$ leads to the pseudo-occupied *k*-SRMOs $\boldsymbol{\varphi}_{\mathrm{p}}^{0,k}$:

$$\begin{aligned}\boldsymbol{\varphi}_{\mathrm{p}}^{0,k} &= \left(\varphi_{\mathrm{p},1}^{0,k} \quad \cdots \quad \varphi_{\mathrm{p},i}^{0,k} \quad \cdots \quad \varphi_{\mathrm{p},n_{\mathrm{p}}^k}^{0,k}\right) \\ &= \boldsymbol{\chi}\mathbf{T}_{\mathrm{p}}^{0,k}.\end{aligned} \tag{50}$$

Appendix 3: Energy subcomponents in Table 2

According to Eq. 1, the energy change arising from three simultaneous X, Y, and Z interactions (XYZ interaction) is

$$E_{\mathrm{XYZ}} = E_{0+\mathrm{XYZ}} - E_0, \tag{51}$$

where $E_{0+\mathrm{XYZ}}$ is the energy of the electronic state with all interaction, including XYZ interaction, activated. Furthermore, the energy component E_{Y} of E_{XYZ}, for instance, is derived from the following equation:

$$E_{\mathrm{Y}} = E_{0+\mathrm{XYZ}} - E_{0+\mathrm{XZ}}. \tag{52}$$

In this equation, $E_{0+\mathrm{XZ}}$ is the energy of the state with all the interaction except Y interaction activated; it, as well as E_0, can be calculated using the state by the SRW method.

References

1. Kitaura K, Morokuma K (1976) Int J Quantum Chem 10:325–340
2. Morokuma K (1977) Acc Chem Res 10:294–300
3. Hayes IC, Stone AJ (1984) Mol Phys 53:69–82
4. Hayes IC, Stone AJ (1984) Mol Phys 53:83–105
5. Stevens WJ, Fink WH (1987) Chem Phys Lett 139:15–22
6. Chen W, Gordon MS (1996) J Phys Chem 100:14316–14328
7. Bagus PS, Hermann K, Bauschlicher CW (1984) J Chem Phys 80:4378–4386
8. Bagus PS, Illas F (1992) J Chem Phys 96:8962–8970
9. Glendening ED, Streitwieser A (1994) J Chem Phys 100:2900–2909
10. Schenter GK, Glendening ED (1996) J Phys Chem 100:17152–17156
11. Glendening ED (2005) J Phys Chem A 109:11936–11940
12. Jeziorski B, Moszynski R, Szalewicz K (1994) Chem Rev 94:1887–1930
13. Moszynski R, Heijmen TGA, Jeziorski B (1996) Mol Phys 88:741–758
14. Dapprich S, Frenking G (1995) J Phys Chem 99:9352–9362
15. Frenking G, Förhlich N (2000) Chem Rev 100:717–774
16. Frenking G, Wichmann K, Förchlich N, Grobe J, Golla W, Le Van D, Krebs B, Läge M (2002) Organometallics 21:2921–2930
17. Frenking G (2005) Science 310:796–797
18. Mochizuki Y, Fukuzawa K, Kato A, Tanaka S, Kitaura K, Nakano T (2005) Chem Phys Lett 410:247–253
19. Khaliullin RZ, Cobar EA, Lochan RC, Bell AT, Head-Gordon M (2007) J Phys Chem A 111:8753–8765
20. Foster JP, Weinhold F (1980) J Am Chem Soc 102:7211–7218
21. Korchowiec J, Uchimaru T (2000) J Chem Phys 112:1623–1633
22. Silva P, Korchowiec J (2011) J Comput Chem 32:1054–1064
23. Fransisco E, Pendás AM, Blanco MA (2006) J Chem Theory Comput 2:90–102
24. Pendás AM, Blanco MA, Fransisco E (2007) J Comput Chem 28:161–184
25. Liu S (2007) J Chem Phys 126:244103-1–244103-5
26. Liu S, Govind N, Pedersen LG (2008) J Chem Phys 129:094104-1–094104-10
27. Tiana D, Francisco E, Blanco MA, Macchi P, Sironi A, Pendás AM (2010) J Chem Theory Comput 6:1064–1074
28. Zieglar T, Rauk A (1977) Theor Chem Acta 46:1–10

29. Mitoraj MP, Michalak A, Ziegler T (2009) J Chem Theory Comput 5:962–975
30. Mo Y, Peyerimhoff SD (1998) J Chem Phys 109:1687–1697
31. Mo Y, Zhang Y, Gao J (1999) J Am Chem Soc 121:5737–5742
32. Mo Y, Schleyer PVR, Wu W, Lin M, Zhang Q, Gao J (2003) J Phys Chem A 107:10011–10018
33. Mo Y, Wu W, Song L, Lin M, Zhang Q, Gao J (2004) Angew Chem 116:2020–2024
34. Mo Y, Gao J, Peyerimhoff SD (2000) J Chem Phys 112:5530–5538
35. Mo Y, Gao J (2000) J Chem Phys A 104:3012–3020
36. Mo Y, Subramanian G, Gao J, Ferguson DM (2002) J Am Chem Soc 124:4832–4837
37. Mo Y, Song L, Wu W, Zhang Q (2004) J Am Chem Soc 126:3974–3982
38. Gianinetti E, Raimondi M, Tornaghi E (1996) Int J Quantum Chem 60:157–166
39. Fornili A, Sironi M, Raimondi M (2003) J Mol Struct (Theochem) 632:157–172
40. Sironi M, Genoni A, Civera M, Pieraccini S, Ghitti M (2007) Theor Chem Acc 117:685–698
41. Brown EC, Bader RFW, Werstiuk NH (2009) J Phys Chem A 113:3254–3265
42. Zhang Y, Wasserman A (2010) J Chem Theory Comput 6:3312–3318
43. Yamada K, Koga N (2007) Frontiers of computational science: proceedings of the international symposium on frontiers of computational science 2005. Springer, Berlin
44. Edmiston C, Rudenberg K (1963) Rev Mod Phys 35:457–465
45. Boys SF (1966) In: Löwdin PO (ed) Quantum theory of atoms, molecules, and solid state. Academic Press, New York
46. Pipek J, Mezey PG (1989) J Chem Phys 90:4916–4926
47. Reed AE, Weinhold F (1985) J Chem Phys 83:1736–1740
48. Tsuzuki S, Tanabe K (1991) J Chem Soc Perkin Trans 2:1255–1260
49. Wiberg KB, Breneman CM (1992) J Am Chem Soc 114:831–840
50. Lauvergnat D, Hiberty PC (1997) J Am Chem Soc 119:9478–9482
51. Kieninger M, Suhai S (1996) J Mol Struct 375:181–188
52. Breneman CM, Wiberg KB (1990) J Comput Chem 11:361–373
53. Wiberg KB, Rablen PR (1995) J Am Chem Soc 117:2201–2209
54. Laidig KE, Cameron LM (1993) Can J Chem 71:872–879
55. Laidig KE, Cameron LM (1996) J Am Chem Soc 118:1737–1742
56. Kemnitz CR, Loewen MJ (2007) J Am Chem Soc 129:2521–2528
57. Fogarasi G, Szalay PG (1997) J Phys Chem A 101:1400–1408
58. Ou M-C, Chu S-Y (1995) J Phys Chem 99:556–562
59. Sandstrom J (1967) J Phys Chem 71:2318–2325
60. Stewart WE, Siddall TH III (1970) Chem Rev 70:517–551
61. Ou M-C, Tsai M-S, Chu S-Y (1994) J Mol Struct (Theochem) 310:247–254
62. Chen W, Gordon MS (1996) J Chem Phys 105:11081–11090
63. Olsen LF, Li Y, Houk KN, Kresge AJ, Schaad LJ (1995) J Am Chem Soc 117:2992–2997
64. Oie T, Topol IA, Burt SK (1995) J Phys Chem 99:905–915
65. Wang X-C, Facelli JC, Simons J (1993) Int J Quantum Chem 45:123–132
66. Burton NA, Chiu SS-L, Davidson MM, Green DVS, Hillier IH, McDouall JJW, Vincent MA (1993) J Chem Soc, Faraday Trans 89:2631–2635
67. Taha AN, Crawford SMN, True NS (1998) J Am Chem Soc 120:1934–1935
68. Taha AN, True NS (2000) J Phys Chem A 104:8609–8616
69. Frisch MJ et al (2004) Gaussian 03, E.01, Gaussian, Inc. Wallingford, CT (see Supporting Information for details)
70. Glendening ED, Reed AE, Carpenter JE, Weinhold F, NBO version 3.1
71. Ditchfield R, Hehre WJ, Pople JA (1971) J Chem Phys 54:724–728
72. Hehre WJ, Ditchfield R, Pople JA (1972) J Chem Phys 56:2257–2261
73. Francl MM, Pietro WJ, Hehre WJ, Binkley JS, Gordon MS, DeFrees DJ, Pople JA (1982) J Chem Phys 77:3654–3665
74. Fujimoto H, Yamasaki T, Mizutani H, Koga N (1985) J Am Chem Soc 107:6157–6161
75. Yamaki D, Nagao H, Yamaguchi K (2001) Int J Quantum Chem 85:204–213
76. Michalak A, Mitoraj M, Ziegler T (2008) J Phys Chem A 112:1933–1939
77. Clark T, Chandrasekhar J, Spitznagel GW, Schleyer PVR (1983) J Comp Chem 4:294–301
78. McLean AD, Chandler GS (1980) J Chem Phys 72:5639–5648
79. Raghavachari K, Binkley JS, Seeger R, Pople JA (1980) J Chem Phys 72:650–654
80. Schmidt MW, Baldridge KK, Boatz JA, Elbert ST, Gordon MS, Jensen JH, Koseki S, Matsunaga N, Nguyen KA, Su SJ, Windus TL, Dupuis M, Montgomery JA Jr (1993) J Comput Chem 14:1347–1363
81. Reed AE, Weinhold F (1983) J Chem Phys 78:4066–4073
82. Reed AE, Weinstock RB, Weinhold F (1985) J Chem Phys 83:735–746